Available online at www.sciencedirect.com

SciVerse ScienceDirect

Scripta Materialia 68 (2013) 773–776

Scripta MATERIALIA

www.elsevier.com/locate/scriptamat

# Fatigue deformation of microsized metallic glasses

Dongchan Jang,[a,*] Robert Maaß,[a] Gongyao Wang,[b] Peter K. Liaw[b] and Julia R. Greer[a,c]

[a]*Department of Applied Physics and Materials Science, California Institute of Technology, Pasadena, CA 91125, USA*
[b]*Department of Materials Science and Engineering, The University of Tennessee, Knoxville, TN 37996, USA*
[c]*The Kavli Nanoscience Institute, California Institute of Technology, Pasadena, CA 91125, USA*

Received 23 October 2012; revised 4 December 2012; accepted 9 December 2012
Available online 20 December 2012

Metallic glasses typically exhibit high strength and a high elastic limit but suffer from poor fatigue resistance. This work demonstrates that 1.6 micron diameter Zr-based metallic glass samples subjected to compressive fatigue cycling did not fail after $40 \times 10^6$ cycles. The fatigue endurance limit was shown to increase to more than 110% of bulk yield strength under compression–compression and up to 90% under bending; those of the same material with macroscopic dimensions are typically at 50% of bulk yield strength.


*Keywords:* Fatigue test; Fatigue; Metallic glass; Focused ion beam (FIB)

During the last decade, metallic glasses have shown promise as candidates for next-generation structural materials because of their concurrent high strengths and high elastic limits, as well as their corrosion resistance [1]. However, the limited amount of post-elastic deformability, which can lead to sudden and catastrophic material failure, has prevented their widespread use in commercial applications. Brittle failure in metallic glasses occurs by the formation of highly localized shear regions, also known as shear bands, when subjected to mechanical loading. Many metallic glasses also exhibit poor fatigue properties, with typical tensile fatigue endurance limits at ~10% of their strength [2,3]. Even under monotonic loading, considerable efforts have been dedicated to preventing metallic-glass-based material systems from forming instabilities, which lead to catastrophic failure [4–6]. For example, 100 nm sized Zr-based metallic glasses have been shown to attain ~25% enhancement in tensile ductility [7,8]. Such a sample size reduction may also offer an opportunity to enhance the fatigue resistance of metallic glasses because the combination of high strength and ductility facilitates greater fracture toughness, which is directly correlated with the materials' resistance to fatigue cracking.

We report compression–compression and bending fatigue experiments on $Zr_{50}Cu_{40}Al_{10}$ cylinders 1.6 microns in diameters and ~4.5 microns high. These samples exhibited a compressive fatigue endurance limit of 2.0 GPa, which is 10% greater than the bulk yield strength. Cycling under bending, which contained a tensile straining component, led to an endurance limit of 1.6 GPa, which is 10% lower than the bulk yield strength. These microsamples did not fail even after $40 \times 10^6$ cycles at applied stresses below these endurance limits. Exceeding the endurance limit even marginally resulted in the immediate sample failure. These observations suggest that micron-sized metallic glasses possess improved fatigue-failure resistance.

Figure 1 depicts the experimental setup for the fatigue experiments: Figure 1a schematically illustrates the load cell and the displacement gauge inside the nanoindenter. Applied load and pillar-length-change data as a function of time are shown in Figure 1b, which also contains a snapshot of the dynamic load signal. Prior to the fatigue experiments, several vertical and slanted samples were deformed quasi-statically to determine their strengths and deformation modes. Figure 2c and f shows the data and the scanning electron microscopy (SEM) images of the micropillars subjected to such monotonic loading: compression (a–c) and bending (d–f). Severe localization into shear bands (Fig. 2b) and pronounced strain bursts upon yielding (Fig. 2c) indicated that these micropillars deformed virtually identically to bulk with their mean compressive yield strengths of 2.04 GPa exceeding bulk by 10% [9–11]. This smaller-is-slightly-stronger trend is consistent with literature for Zr-based metallic glasses

* Corresponding author. Tel.: +1 626 395 6233; e-mail: jangd@caltech.edu

1359-6462/$ - see front matter © 2012 Acta Materialia Inc. Published by Elsevier Ltd. All rights reserved.
http://dx.doi.org/10.1016/j.scriptamat.2012.12.011

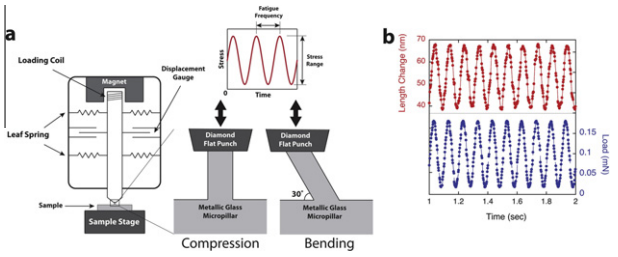


**Figure 1.** (a) Schematic illustration of apparatus and specimens for fatigue experiments. (b) Typical length change and load data as a function of time.

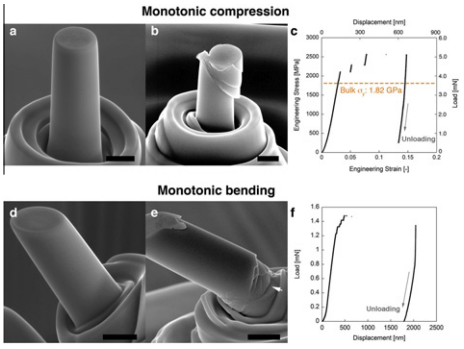


**Figure 2.** SEM images of the typical (a) as-fabricated and (b) deformed metallic glass micropillar for monotonic uniaxial compression and (c) corresponding engineering stress–strain curve. SEM images of the typical as-fabricated (d) and deformed (e) metallic glass micropillar for monotonic bending and (f) corresponding load–displacement curve. The arrow in (e) indicates a crack. All scale bars in the SEM images are 1 micron long.

[7,12]. The load–displacement data for the bending experiments (Fig. 2f) exhibited more stable plasticity as compared with compressive testing (Fig. 2c). This is likely a result of the non-uniform stress distribution within the bending sample, where the driving force for shear-band propagation vanishes as it approaches the neutral axis. The massive shear-band agglomerate at the bottom of the micropillar indicates a high stress concentration in that region. The crack visible on the top surface near the base of the bent micropillar (indicated in Fig. 2e) verified that crack-opening tensile stresses were generated as a result of bending.

Figure 3 summarizes the results from the compression and bending fatigue experiments on $Zr_{50}Cu_{40}Al_{10}$ metallic glass micropillars. The plot in Figure 3a displays all of the explored fatigue conditions with previously published tension–tension stress and fatigue-life data (also known as the S–N curve) of the same glass with dimensions more than ~1000×larger than studied here, shown for comparison (triangular-shaped data points) [11]. Data points from this work correspond to the test conditions that were applied/reached and do not represent the fatigue life under a given stress as in the S–N curve, with the exception of two cases (open diamonds in Fig. 3a). The remaining 18 metallic glass micropillars remained intact up to at least $20 \times 10^6$ cycles under compression–compression loading even at the maximum applied stress ($\sigma_{max}$) of 110% of bulk yield strength ($\sigma_y = 1820$ MPa) [11]. Exceeding the applied

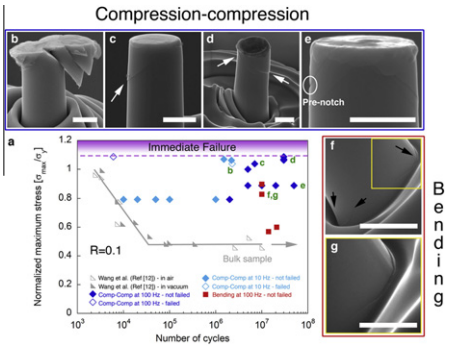


**Figure 3.** (a) Plot displaying all the experimental conditions of current study together with S–N data from bulk metallic glass of the same composition ([11]). (b)–(g) SEM images of selected micropillars after fatigue experiments. The test conditions for the SEM images in (b)–(f) correspond to the data points with the same letter in (a). The SEM image in (g) shows the magnified region within the square in (f). The scale bars in (b)–(f) are 1 micron long and the one in (g) is 500 nm long.

stress over $1.1\sigma_y$ resulted in immediate sample failure. In bending experiments, where parts of the pillar experienced tensile stresses, the threshold for immediate failure was $0.9\sigma_y$. No micropillars failed below $10 \times 10^6$ cycles during bending-fatigue experiments at the maximum applied stresses below $0.9\sigma_y$. The S–N curve for previously reported macroscopic samples in Figure 3a corresponds to tension–tension loading, which has a two orders of magnitude lower fatigue lifetime than that under compresson–compression modes. However, a recent study on a glass similar to the one studied in this work revealed that the influence of loading direction on the fatigue endurance limit was marginal [13,14], which suggests that the improvement in fatigue endurance limit observed in this work likely stems from other factors.

The asymmetry in the fatigue threshold between compression and bending may be caused by the complex stress concentration at the base of the slanted micropillars in the latter. Utilizing rigid boundary condition at the pillar base (Fig. 1a), the elastic stresses and strains within the bent pillar were estimated using an analytical solution of the form: $\sigma_{ten} = [8(L/D)\sin\theta - \cos\theta](4P/\pi D^2)$, where $\sigma_{ten}$ is the maximum tensile stress at the pillar base, $L$ and $D$ are pillar height and diameter, respectively, and $\theta$ is the inclination angle of the pillar to the loading axis. This assumption leads to an over-estimation of the stress because the exposure to Ga ion bombardment during FIB-based fabrication process likely weakens the pillar–substrate interface. Data corresponding to bending experiments (red solid squares in Fig. 3a) was approximately calculated as the ratio between the maximum load, $L_{max}$ and the load at the onset of yielding, $L_y$, determined from the monotonic bending experiments on the slanted pillars. This avoids the complication of accounting for the pillar base–substrate compliance.

Figure 3b–g displays the SEM images of several fatigued micropillars. The testing conditions in each image correspond to the data points denoted by the same indices in Figure 3a. These images reveal that even when the micropillars did not experience catastrophic failure, multiple non-catastrophic shear bands were formed, as

indicated by the arrows on the images in Figure 3c, d and f. These diffuse shear bands were stable in the course of the fatigue loading and never developed into fully transecting, catastrophic shear bands or cracks. It is likely that the local stress concentrators, caused by the top and bottom constraints during the experiment, incited the nucleation of such non-catastrophic shear bands because they were mostly formed near the micropillar top in the compression experiments and at the pillar base in the bending experiments. The post-mortem image of the sample that failed by compressive fatigue cycling (Fig. 3b) reveals a morphology very similar to that of the quasi-statically compressed sample (Fig. 2b). These are in contrast to the typically observed post-fatigue signature in BMGs, characterized by fatigue striations and vein-like morphology [2,11,15]. Experiments on additional samples, which were fabricated to contain sharp notches carved roughly halfway along the pillar height showed identical shear-band-ridden morphologies and enhanced fatigue performance as the un-notched specimens (Fig. 3e).

Fatigue failure of BMGs has been reported to occur in stages [15,2,16]. Damage initiation usually begins by diffuse shear-band formation or the development of mixed-mode microcracks emanating from stress concentrators, such as pores, surface flaws and sample edges [15,2]. Subsequently, additional cracks originate from those shear bands [16], which has been shown to lead to catastrophic failure once the critical crack size is attained [15,2,16]. In crystalline metals, the initial damage-initiation phase usually represents the most time-consuming process: the duration of the stable initial fatigue stage has been reported to last nearly 80% of the total fatigue lifetime, which in part is the reason for the high resistance of metals and alloys to fatigue damage [14,17]. Conversely, the low fatigue endurance limit of ~0.1–0.5 in Zr-based BMGs has been attributed to the combination of early onset and the short duration of the damage initiation phase, which resulted in rapid material failure. SEM images of the post-fatigued micro-sized glasses, studied in this work (Fig. 3), clearly illustrate that initially formed diffuse shear bands rarely evolved into full shear bands or cracks.

It is unlikely that the suppression of catastrophic failure in these dynamically tested small-scale metallic glasses was caused by the absence of tensile crack-opening stresses under compression–compression loading because a similar fatigue resistance was observed in bending, where the local tensile stresses were estimated to be sufficiently high to initiate shear-banding and microcracking (Fig. 3f and g). Further, a similar glass as investigated in the current study but with macroscale dimensions failed after $\sim 1 \times 10^5$ cycles under a similar compression–compression loading schedule [13,14]. Our experiments also revealed that surface flaws such as intentionally fabricated notches and mechanically induced shear-band offsets did not alter the fatigue endurance limit (Fig. 3a). This implies that the improved fatigue resistance cannot be explained in terms of the weakest-link (Weibull) statistics.

We propose that the physical foundation for the amplified fatigue resistance offered by the small-scale metallic glasses is related to two characteristic length scales associated with these amorphous solids: the characteristic atomic-level scale and the mesocopic length-scale of shear-band kinetics. The transformation of the initially formed shear bands into cracks in cyclically strained BMGs has been explained by the coalescence of free volume within the shear bands into voids [18,3]. Molecular dynamics (MD) simulations suggest that in small-scale metallic glasses, structural atomic rearrangements and dynamic recovery are favored over the free volume coalescence during cyclic loading because of a constant interconversion between locally rigid and locally soft atomic clusters, which inhibits the overall structural change [19,20]. The dynamic recovery and structural reorganization at the atomic scale have also been shown to reduce the number of alpha and beta relaxations with low transition energies, which caused the yield strengths of the fatigued microsamples to be greater than those of the unstrained samples [21]. The quasi-static compression experiments on the fatigued micropillars performed in this work revealed a 5% increase in the yield strength, consistent with this framework.

Shear banding is a three-step process comprised of initiation, propagation and, in some cases, arrest [22–24]. The initiation typically occurs on the order of microseconds (Fig. 4a), during which a stress-induced dilatational transformation towards a lower packing density generates a planar defect that can mediate plastic strain thereafter [22]. The subsequent propagation of the shear band either continuously accelerates, which leads to imminent catastrophic failure, or first accelerates and then decelerates until stopping, which results in stable flow (Fig. 4c) [24,23]. We hypothesize that high-frequency sinusoidal fatigue loading, which was applied to the micropillars in this work, may have limited the ability of shear bands to effectively propagate via either one of these mechanisms because of the deficient duration of the sufficiently high stresses necessary for their motion (Fig. 4d). If the duration of each pulse, $t_f$, is significantly shorter than the time scale for the shear-band propagation, $t_p$, then the applied stress that is sufficiently large to cause shear-band initiation or

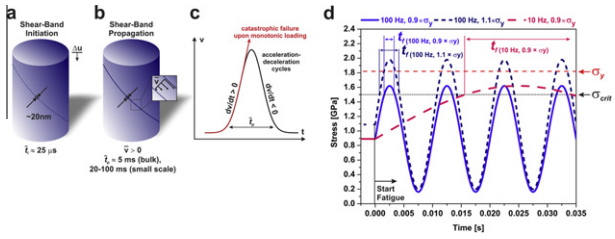


**Figure 4.** (a) At some critical stress, $\sigma_{crit}$, which may be lower than the yield stress, $\sigma_y$, a shear band is initiated within a few tens of microns. At this stage the ~20 nm thick planar defect remains stationary. (b) Subsequently, the shear band propagates for a time $t_p$ at a size-dependent mean velocity $v$. (c) In some metallic glasses continuous shear-band acceleration is observed, which leads to catastrophic failure, whereas other glasses exhibit shear deceleration, which allows for intermittent stable plastic flow. (d) Upon cyclic loading, the stress attains values above $\sigma_{crit}$ during a frequency- and peak-load-dependent time $t_f$. If $t_f < 0.5 \times t_p$, the time spent at or above $\sigma_{crit}$ is not sufficient to allow catastrophic shear-band propagation for a brittle glass.

reactivation does not last long enough for it to propagate, which suppresses catastrophic failure via autocatalytic acceleration. At such cycling frequencies, every shear band that forms would remain stable. $t_p$ have been reported to be on the order of milliseconds for Zr-based BMGs at ambient condition (Fig. 4b) [23]. The previously reported $t_p$ of 5 ms provides a conservative bound for $t_p$, which was shown to increase to 20–100 ms in Cu-based metallic glasses when the sample size was reduced to the micron and nanometer scales [25]. We hypothesize that the the shear-band propagation time in the small-scale metallic glass samples studied here exceeds $t_f$ at all studied fatigue frequencies, which drives a longer fatigue life by suppressing shear-band propagation and subsequent run-away failure.

In summary, compression–compression and bending-fatigue experiments performed on $Zr_{50}Cu_{40}Al_{10}$ metallic glass cylinders 1.6 microns in diameter and 4.5 microns high revealed an improvement in the fatigue endurance limit by a factor of 2 as compared to the same glass with macroscopic dimensions of 2.98 mm in diameter. Their endurance limit was elevated to 110% and to 90% of the bulk yield strength, for compression and bending, respectively. At a maximum compressive stress of 90% of the bulk yield strength, all of the samples sustained more than 40 million cycles without failure. The observed combination of a compressive fatigue endurance limit of ~1 and a yield strength of ~2 GPa offered by the small-scale metallic glasses uniquely places these materials in a previously unattainable material property space, opening new routes in miniaturization and reliability of micro- and nanodevice engineering.

D.J., R.M. and J.R.G. gratefully acknowledge the financial support of Office of Naval Research (N00014-09-1-0883). R.M. also acknowledges the financial support of the Alexander von Humboldt foundation, as well as his Humboldt host G.M. Pharr. G.W. and P.K.L. also acknowledge the financial support from National Science Foundation (DMR-0909037, CMMI-0900271, and CMMI-1100080). The authors also acknowledge critical support and infrastructure provided for this work by the Kavli Nanoscience Institute at Caltech. The authors thank Prof. Yokoyama of Tohoku University for providing the bulk sample and Prof. William L. Johnson at Caltech for useful discussion.

[1] C.A. Schuh, T.C. Hufnagel, U. Ramamurty, Acta Materialia 55 (12) (2007) 4067–4109, http://dx.doi.org/10.1016/j.actamat.2007.01.052.
[2] B. Menzel, R.H. Dauskardt, Acta Materialia 54 (4) (2006) 935–943, http://dx.doi.org/10.1016/j.actamat.2005.10.021.
[3] G. Wang, P.K. Liaw, M. Morrison, Intermetallics 17 (8) (2009) 579–590, http://dx.doi.org/10.1016/j.intermet.2009.01.017.
[4] D.C. Hofmann, J.-Y. Suh, A. Wiest, G. Duan, M.-L. Lind, M.D. Demetriou, W.L. Johnson, Nature 451 (7182) (2008) 1085–1089, http://dx.doi.org/10.1038/nature06598.
[5] M.D. Demetriou, M.E. Launey, G. Garrett, J.P. Schramm, D.C. Hofmann, W.L. Johnson, R.O. Ritchie, Nature Materials 10 (February) (2011) 123–128, http://dx.doi.org/10.1038/nmat2930.
[6] J.-Y. Kim, D. Jang, J.R. Greer, Advanced Functional Materials 21 (23) (2011) 4550–4554, http://dx.doi.org/10.1002/adfm.201101164.
[7] D. Jang, C.T. Gross, J.R. Greer, International Journal of Plasticity 27 (6) (2011) 858–867, http://dx.doi.org/10.1016/j.ijplas.2010.09.010.
[8] D. Jang, J.R. Greer, Nature Materials 9 (3) (2010) 215–219.
[9] Y. Yokoyama, K. Fukaura, A. Inoue, Materials Transactions 45 (5) (2004) 1672–1678, http://dx.doi.org/10.2320/matertrans.45.1672.
[10] Y. Yokoyama, P.K. Liaw, M. Nishijima, K. Hiraga, R.A. Buchanan, A. Inoue, Materials Transactions 47 (5) (2006) 1286–1293, http://dx.doi.org/10.2320/matertrans.47.1286.
[11] G. Wang, P.K. Liaw, Y. Yokoyama, A. Inoue, C.T. Liu, Materials Science and Engineering: A 494 (1-2) (2008) 314–323, http://dx.doi.org/10.1016/j.msea.2008.04.034.
[12] Y. Lai, C.J. Lee, Y. Cheng, H. Chou, H. Chen, X. Du, C. Chang, J. Huang, S. Jian, J. Jang, Scripta Materialia 58 (10) (2008) 890–893, http://dx.doi.org/10.1016/j.scriptamat.2008.01.009.
[13] G. Wang, D. Qiao, Y. Yokoyama, M. Freels, A. Inoue, P.K. Liaw, Journal of Alloys and Compounds 483 (1-2) (2009) 143–145, http://dx.doi.org/10.1016/j.jallcom.2008.07.228.
[14] P. Hess, B. Menzel, R.H. Dauskardt, Scripta Materialia 54 (3) (2006) 355–361, http://dx.doi.org/10.1016/j.scriptamat.2005.10.007.
[15] M. Freels, G. Wang, W. Zhang, P.K. Liaw, A. Inoue, Intermetallics 19 (8) (2011) 1174–1183, http://dx.doi.org/10.1016/j.intermet.2011.03.023.
[16] G. Wang, P.K. Liaw, X. Jin, Y. Yokoyama, E.-W. Huang, F. Jiang, L.M. Keer, A. Inoue, Journal of Applied Physics 108 (11) (2010) 113512, http://dx.doi.org/10.1063/1.3501102.
[17] S. Suresh, Fatigue of materials, 1st ed., Cambridge University Press, Cambridge, 1991.
[18] K.K. Cameron, R.H. Dauskardt, Scripta Materialia 54 (3) (2006) 349–353, http://dx.doi.org/10.1016/j.scriptamat.2005.10.006.
[19] Y. Shi, D. Louca, G. Wang, P.K. Liaw, Journal of Applied Physics 110 (2) (2011) 023523, http://dx.doi.org/10.1063/1.3610443.
[20] Y. Lo, H. Chou, Y. Cheng, J. Huang, J. Morris, P.K. Liaw, Intermetallics 18 (5) (2010) 954–960, http://dx.doi.org/10.1016/j.intermet.2010.01.012.
[21] C. Packard, E. Homer, N. Al-Aqeeli, C.A. Schuh, Philosophical Magazine 90 (10) (2010) 1373–1390, http://dx.doi.org/10.1080/14786430903352664.
[22] D. Klaumünzer, A. Lazarev, R. Maaß, F.H. Dalla Torre, A. Vinogradov, J.F. Loffler, Physical Review Letters 107 (18) (2011) 185502, http://dx.doi.org/10.1103/PhysRevLett.107.185502.
[23] R. Maaß, D. Klaumünzer, J.F. Loffler, Acta Materialia 59 (8) (2011) 3205–3213, http://dx.doi.org/10.1016/j.actamat.2011.01.060.
[24] R. Maaß, D. Klaumünzer, G. Villard, P.M. Derlet, J.F. Loffler, Applied Physics Letters 100 (7) (2012) 071904, http://dx.doi.org/10.1063/1.3684871.
[25] C. Chen, Y. Pei, J.T. De Hosson, Acta Materialia 58 (1) (2010) 189–200, http://dx.doi.org/10.1016/j.actamat.2009.08.070.